Measurement of High-Re Turbulent Pipe Flow Using Single-Pixel PIV

G. Oldenziel[1,*], S. Sridharan[2], J. Westerweel[3]

1: Deltares & Delft University of Technology, The Netherlands
2: Dept. Process & Energy, Faculty 3ME Delft University of Technology, The Netherlands
3: Laboratory for Aero & Hydrodynamics Delft University of Technology, The Netherlands
*Corresponding author: gosse.oldenziel@deltares.nl

Keywords: PIV processing, turbulence, pipe flow

ABSTRACT

In this paper we present PIV measurements of turbulent pipe flow at Reynolds numbers between 3.4×10^5 and 6.9×10^5. We apply a so-called 'single-pixel correlation' that yields a superior spatial resolution (Westerweel et al., 2004). We use the location and shape of the averaged correlation peak to obtain the mean velocity and normal and Reynolds stresses (Scharnowski et al., 2012). A novel aspect of the single-pixel correlation approach is the extension to determine the spatial correlation of the velocity fluctuations. In this contribution we present the results for $Re_D = 4.98\times10^5$, corresponding to a shear Reynolds number Re_τ = 10254, with a resolution of Δy^+ = 19.

1. Introduction

One of the main limitations in obtaining experimental data of wall turbulence at very high Reynolds number is the limited spatial resolution, especially in the near-wall region. Intrusive measurement methods, such as Pitot tube and hotwire anemometry, are limited by the dimensions of the probe. Therefore, there has been a drive to design smaller measurement probes ((Vallikivi et al., 2011)). An alternative is to change the scale of the facility relative to the typical dimensions of the probe ((Vinuesa et al., 2016)). Particle image velocimetry (PIV) is a non-intrusive measurement method where commonly the instantaneous flow velocity field is estimated in small interrogations regions ((Adrian & Westerweel, 2011)). The finite dimensions of the interrogation windows, typically 32×32 pixels, limit also the spatial resolution in the near wall region. Using an optical system with a high magnification ((Willert et al., 2017)) obtained detailed measurements in the near-wall region of the CICLoPE facility, although a mirror needed to be introduced into the facility to accommodate the measurements. Another approach is to reduce the spatial resolution of the PIV measurement to a single pixel. This approach was first described for microfluidic applications in (Westerweel et al., 2004), and that was later also applied to measure the mean velocity profile in the near-wall region of a turbulent boundary layer ((Kähler et al., 2006)). The shape of the displacement correlation peak represents the local probability-density function for the displacement that

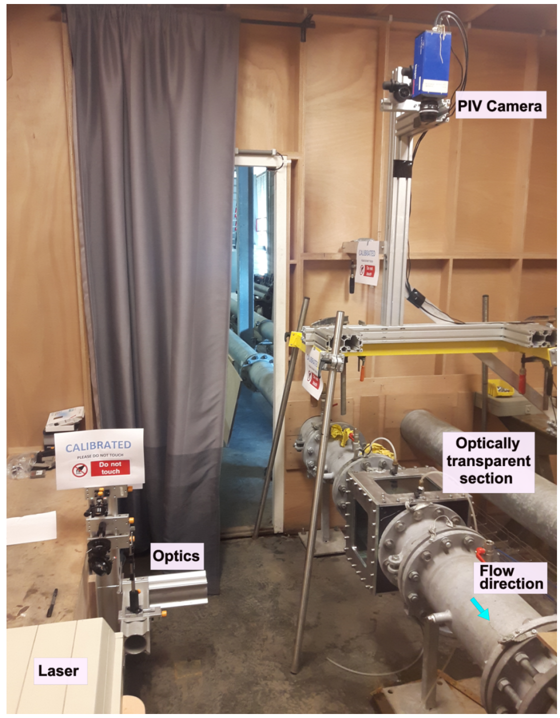

Figure 1. Setup of the PIV system used to measure the flow in the Alpha Loop; from: (Sridharan, 2018).

is convoluted with the particle image self-correlation ((Westerweel, 2008)). This makes it possible to estimate also the normal stresses and Reynolds stress from the measured shape of the correlation peak ((Scharnowski et al., 2012)). However, to fully describe the turbulent flow statistics, it is necessary to also measure the local length scales. In this paper, we present a further extension to estimate the local spatial correlation of the velocity fluctuations that is based on the single-pixel algorithm.

2. Experimental Set-Up

We demonstrate this approach by measuring the turbulent flow in the 'Alpha Loop' at Deltares (Delft, The Netherlands); see Figure 1. This facility is a closed-loop water-filled pipe with a length of 320 m and a diameter of 206 mm. The flow loop is intended for industrial-scale testing of multiphase flows. In Figure 2 we show the friction coefficients based on the measured pressure gradient and measured bulk flow rate. The inset of Figure 2 shows that the pipe has a small roughness of $k_s/D = 3{\cdot}10^{-5}$, corresponding to $k_s = 6.2\,\mu m$. For the PIV measurements the pipe was fitted with a transparent test section (made of PMMA) enclosed in a rectangular transparant water-filled box that can withstand the operating pressure (3 bar) and avoids serious light refraction from the curved pipe wall; a special arrangement of slits reduced internal reflections of the light sheet from the recorded images ((Sridharan, 2018)). The flow was seeded with 10 μm diameter tracer particles (Sphericel 110P8, Potters Industries Inc.). The flow was illuminated with a 0.8 mm thick light sheet generated from the beam of a double-pulsed dual Nd:YAG laser. Images were

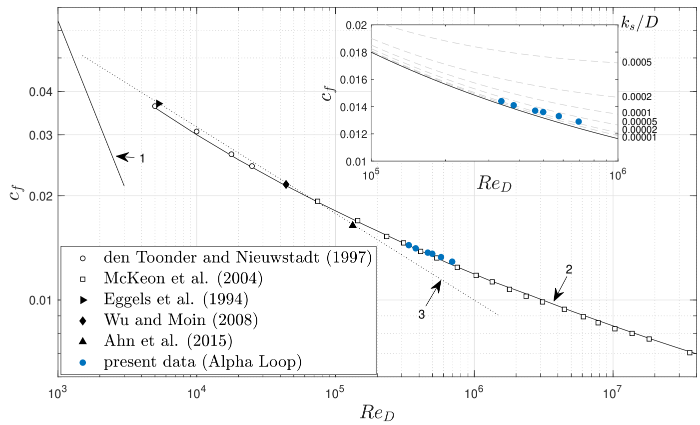

Figure 2. Friction factor as measured and simulated in different pipe flow facilities as a function of the Reynolds number Re_D. The lines represent: 1 the friction factor for laminar Poiseuille flow ($c_f = 64/\mathrm{Re}_D$); 2 the friction law for a smooth wall, (Zagarola & Smits, 1998); 3 the Blasius friction law ($c_f = 0.316\mathrm{Re}_D^{-1/4}$). Experimental and numerical data from: Eggels et al. (1994), Wu & Moin (2008), Ahn et al. (2015), den Toonder & Nieuwstadt (1997), McKeon et al. (2004) and present data. The inset shows the present data along with lines for different values of the relative roughness k_s/D according to the correlation of Colebrook (1939). The present data agrees with $k_s/D = 0.00003$, leading to $k_s = 6.2\ \mu$m.

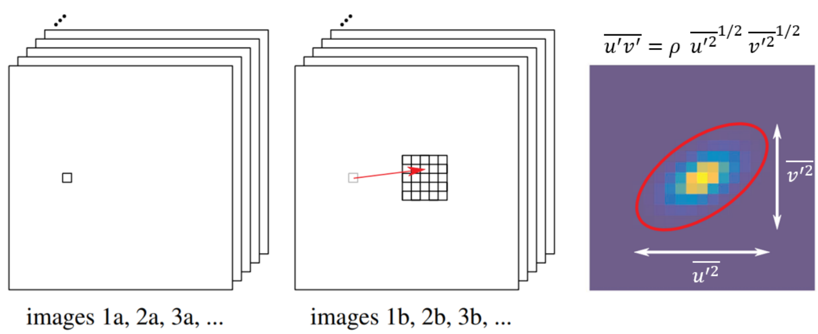

Figure 3. Principle of single-pixel PIV. For a set of image pairs the intensity at a given pixel location in the first exposure is correlated over a small region in the second exposure. The velocity is determined from the location of the displacement-correlation peak. The shape and orientation of the correlation peak yields $\overline{u'^2}$, $\overline{v'^2}$, and $\overline{u'v'}$.

recorded using a CCD camera (SensiCam QE, 1376×1040 pixels with 6.45 μm pixel pitch) equipped with a 50 mm lens (Micro Nikkor) using a f/4 aperture stop. The image magnification was $M_0 = 0.035$, ensuring ample focal depth and diffraction-limited particle images of 5.4 μm diameter. The recorded images were pre-processed using a 5×5-px minmax filter ((Adrian & Westerweel, 2011)) to enhance the image contrast and to reduce the number of spurious vectors by a factor of 4-6. Remnants of the internal reflections, which occur as thin horizontal lines near the pipe walls, were removed using a Fourier filter, similar to the method for removing striations in LIF images ((Westerweel et al., 2011)).

3. Single-pixel correlation

The conventional PIV method determines the local instantaneous particle-image displacement by computing the spatial correlation in typically 32×32-pixel interrogation windows and identifying the location of the displacement-correlation peak; the velocity is obtained by dividing the particle-image displacement by the exposure time-delay between the two laser light pulses that illuminate the flow ((Adrian & Westerweel, 2011)). Alternatively, the particle-image displacement can be found by correlating a single pixel in the first image frame with pixels in a small domain in the second frame, and summing the correlations over many frame pairs; see Figure 2. When one uses 1024 frames, in principle the same amount of information is processed as for a single 32×32-pixel (=1024 pixels) interrogation window. The gain is that the spatial resolution is now determined by the dimension of a single pixel, at the cost of losing the ability of recording time-resolved flows. This is attractive for stationary laminar and turbulent flows where a high spatial resolution is required. When the correlation is averaged over a sufficient number of frame pairs, it is possible to extract the normal and Reynolds stresses from the shape and orientation of the displacement-correlation peak ((Scharnowski et al., 2012)). A two-dimensional Gaussian distribution is fitted to the displacement-correlation peak, which is corrected for the convolution with the particle-image self-correlation, and the normal and Reynolds stresses are obtained from the moments of the peak; see Figure 3. In this paper we introduce an extension to the single-pixel approach, and that is the evaluation of spatial correlations of the velocity fluctuations, see Figure 4. This is achieved by constructing the joint probability density function of the velocity fluctuations at two distinct points (x_1, x_2) in the flow. Each single-pixel correlation for an individual frame pair is an estimate of the probability density function (pdf) $f(u, v|x)$. When we multiply the pdf's at two distinct positions, we obtain an estimate of the joint probability density function $f(u_1, v_1, u_2, v_2|x_1, x_2)$. We now simplify this, by considering a projection of the joint pdf for only one velocity component, i.e. $f(u_1, u_2|x_1, x_2)$. By averaging over a substantially large number of frame pairs, and making use of any homogeneous direction in the flow (here the axial flow direction), we can obtain a converged result from which we can estimate the spatial correlation: $R_{uu}(\Delta x) = \overline{u'(x)u'(x + \Delta x)}$.

4. Results

For each Reynolds number a total of 20,000 double-frame images were recorded. Here we present mainly results obtained at $Re_D = 4.98 \times 10^5$. The corresponding shear Reynolds number Re_τ is 10,254. The spatial resolution of the conventional PIV is given by the dimensions of the 32×32-pixel interrogation window. For the measurement presented here this corresponds to a resolution of $\Delta y^+ \cong 600$. Evidently, this is too crude to make measurements in the near-wall region. The single-pixel approach gives a measurement at each (radial) pixel location, and thus gives a spatial resolution of Δy^+ = 19. This would in principle be sufficient to determine the flow profiles in the entire log-region. Figure 5 shows the measured velocity profiles with both the conventional and the single-pixel PIV approaches. The conventional PIV was performed over the entire flow, while

$$R_{uu}(\Delta x) = \overline{u'(x)u'(x+\Delta x)} = \overline{u'^2}\rho(\Delta x)$$

$$R_{uu}(\Delta x) = \int u_1 u_2 f(u_1, u_2 \,|\, x_1, x_2) du_1 du_2 \qquad \Delta x = x_2 - x_1$$

$$f(u_1, u_2 \,|\, x_1, x_2) = \sum_i f_1^{(i)}(u_1 \,|\, x_1) \times f_2^{(i)}(u_2 \,|\, x_2)$$

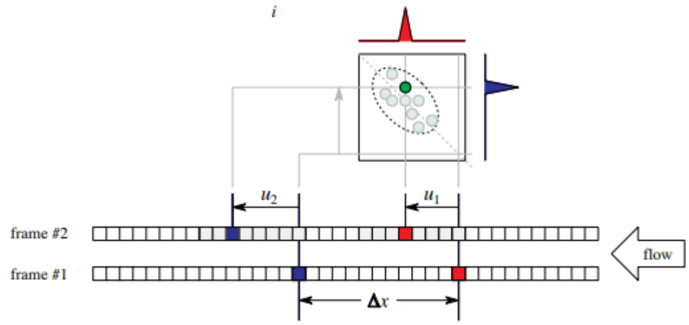

Figure 4. Principle of measuring spatial correlation of the axial velocity fluctuations using single-pixel PIV. The joint probability density function is constructed via multiplication and summation of the suitable correlation functions.

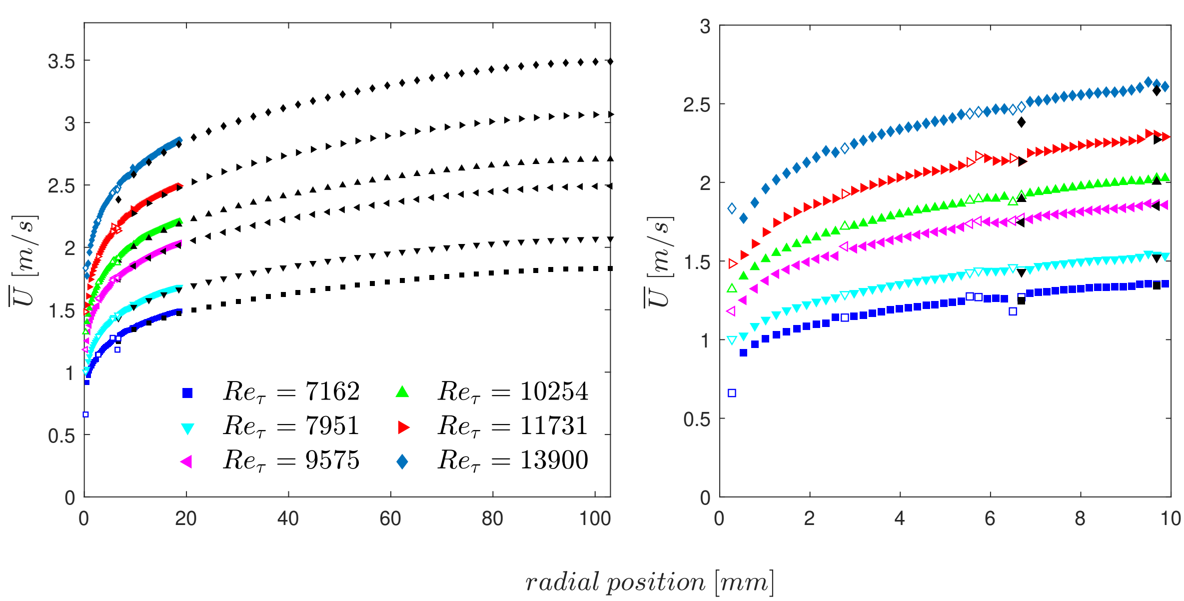

Figure 5. (top) Measured mean axial velocity profile from the wall to the axis of the pipe. Black markers represent the conventional PIV with 32×32-pixel interrogation windows; colored markers are the single-pixel correlation results. (bottom) Detail for the 10 mm region near the wall. Open markers indicate reflection locations or possible influence of the wall.

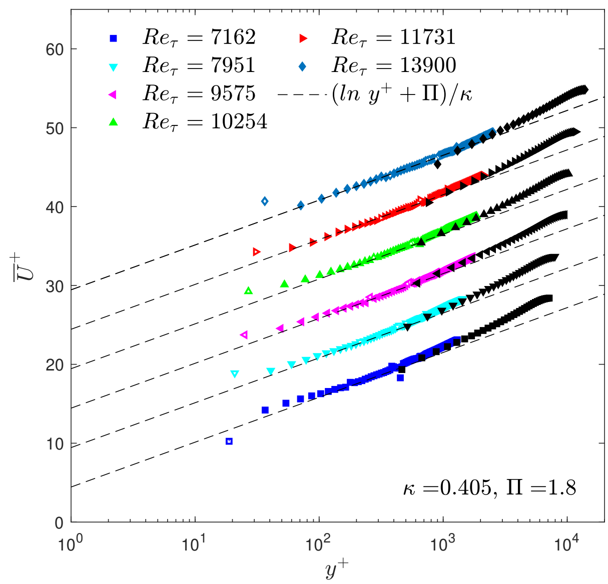

Figure 6. The mean axial velocity profile in wall units for all values of Re_τ. The black markers represent the conventional PIV results using 32×32-pixel interrogation regions; the colored markers represent the single-pixel PIV result. Open markers indicate reflection locations or possible influence of the wall. The dashed lines indicate $(\ln y^+ + \Pi)/k$ where $\Pi = 1.8$ and $k = 0.405$. Lines for increasing values of Re are shifted by 5 plus units.

the single-pixel results were only done for the near wall flow region, and ensuring a sufficient overlap with the conventional PIV data. Figure 6 shows the velocity profiles for all values of Re, but now in a semi-log plot, which illustrates the high level of accuracy of the single-pixel PIV results and the extension of the range in the log-region by a decade in wall units. The profiles coincides with the log profile with a von-Kármán constant of k = 0.405.

Figure 7 shows the results for the normal stresses and the Reynolds stress for $\mathrm{Re}_D = 4.98\times10^5$. The conventional PIV method using 32×32-pixel interrogation windows shows erroneous results for the radial normal stress and the Reynolds stress for $r/D > 0.43$, which corresponds to a distance $y^+ < 10^3$ from the wall. The single-pixel PIV results appears to give reliable results when approaching the wall. The single-pixel PIV results for the Reynolds stress appear to deviate from the surrounding data, which can be attributed to interference of the remaining reflections with the estimate of the displacement correlation peak. One of the features observed in high-Re turbulent pipe flow is the emergence of a so-called 'outer peak' in the streamwise normal stress ((Hultmark et al., 2013), (Willert et al., 2017)).

In Figure 8 we plot the streamwise normal stress in wall units in a semi-log plot. Please note that the inner peak, which is located at $y^+ \approx 10 - 20$, could not be resolved in the single-pixel data. We compare our results with those of (Willert et al., 2017) and those of (Hultmark et al., 2013) taken at almost the same Reynolds number. The results appear to be in agreement for $y^+ > 300$. In the present data the plateau in normal stress is resolved up to $y^+ \approx 150$.

Finally, in Figure 9 we present the results for the spatial correlation R_{uu} of the axial velocity fluc-

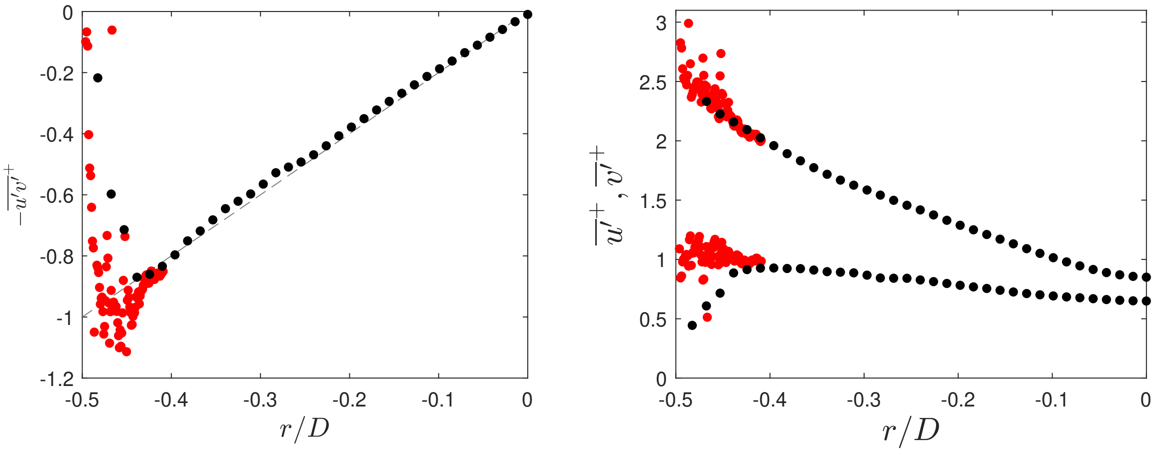

Figure 7. The normal and Reynolds stresses in wall units for $\mathrm{Re}_D = 4.98 \times 10^5$. Top: Reynolds stress $\overline{u'v'}^+$. Bottom: normal stresses $\overline{u'}^+$ and $\overline{v'}^+$ Black dots represent the 32×32 data and red dots represent the single pixel results.

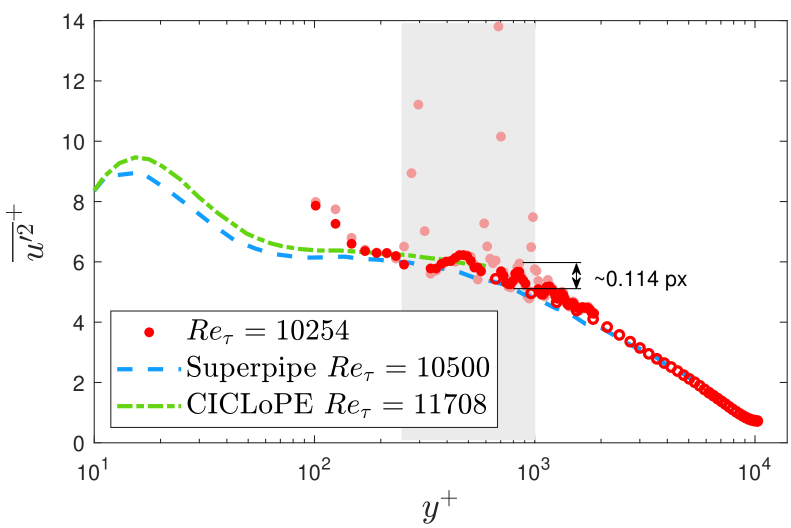

Figure 8. The streamwise normal stress $\overline{u'^2}^+$ as a function of the distance from the wall for Re_τ = 10254 ($\mathrm{Re}_D = 4.98 \cdot 10^5$). The red circles represent the 32×32-px PIV data, the light red dots the single-pixel PIV data and the bright red dots the five point moving median filtered single-pixel PIV data. The grey area indicates locations where the single pixel data is influenced by reflections. The effect of the reflections is counteracted by expanding the number of Fourier modes in the image pre-processing to five for radii $250 < y^+ < 1000$ (the grey area in the figure). The dash-dotted green curve represents the data of (Willert et al., 2017) for $\mathrm{Re}_\tau = 11.7 \cdot 10^3$ and the dashed blue curve represents the data of (Hultmark et al., 2013) for $\mathrm{Re}_\tau = 10.5 \cdot 10^3$.

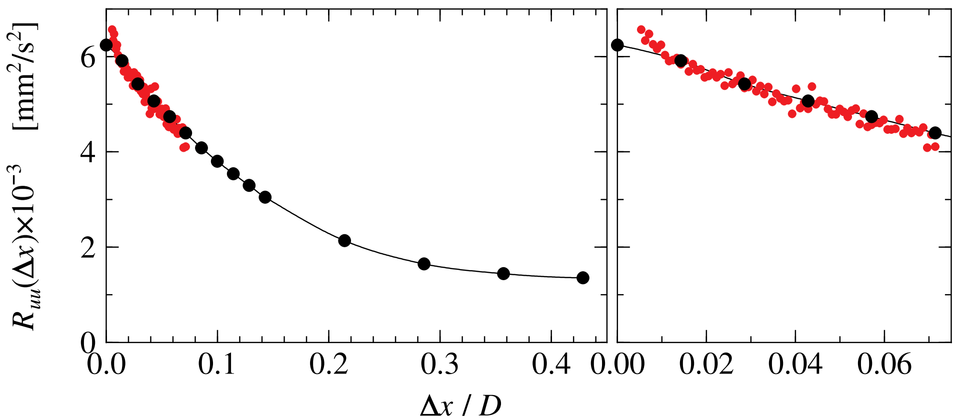

Figure 9. (left) The spatial correlation $R_{uu}(\Delta x)$ of the axial velocity fluctuations at the pipe centerline. Symbols correspond to those in Fig. 7. (right) Detail of $R_{uu}(\Delta x)$ for $\Delta x/D < 0.075$.

tuations at the pipe centerline. Please note the agreement in the shape of the spatial correlation coefficient for the conventional and single-pixel PIV, except for very small separations, where the single-pixel PIV result appears to give a slightly higher correlation. The single-pixel result was normalised to match the tail of the spatial correlation. The difference towards zero offset would indicate the result of the spatial filtering of the conventional PIV analysis. This also demonstrates the potential for single-pixel PIV to estimate the local Taylor micro-scale and dissipation rate for this type of flows from these high-resolution PIV measurements. However, this needs to be further confirmed by analysing the full set of measurements. It should also be noted here that for the computation of each data point in the correlation from the conventional PIV data, we processed 1000 frame pairs with 53 interrogations (with 50% overlap) along the centerline, each with 32×32 pixels, which corresponds to a total of 54×10^6 pixels; the single-pixel result is based on a single 900-px image row of over 9,000 frame pairs, representing a total of 16×10^6 pixels.

5. Conclusions

We present high-resolution PIV results (ultimately limited by the pixel size) of turbulent pipe flow, using a single-pixel PIV approach. This improves the spatial resolution by more that an order of magnitude over conventional PIV methods, while still recording the data over the full pipe diameter. This is applied to an industrial-style pipe flow facility at Deltares, at shear Reynolds numbers between 7,162 and 13,900. The results presented in this abstract are from the measurement at a shear Reynolds number of Re_τ = 10,254. A novel aspect of the work is the extension of single-pixel PIV from single-point to two-point flow statistics, demonstrated by a high-resolution result for the spatial correlation of the axial velocity fluctuations.

References

Adrian, R. J., & Westerweel, J. (2011). *Particle Image Velocimetry*. Cambridge University Press.

Ahn, J. H., J. Lee, Lee, J., Kang, J., & Sung, H. J. (2015). Direct numerical simulation of a 30R long turbulent pipe flow at $\mathrm{Re}_\tau = 3008$. *Phys. Fluids*, *27*, 065110.

Colebrook, C. F. (1939). Turbulent flow in pipes, with particular reference tothe transition region between smooth and rough pipe laws. *J. Inst. C. E.*, *11*, 133-156.

den Toonder, J. M. J., & Nieuwstadt, F. T. M. (1997). Reynolds number effects in a turbulent pipe flow for low to moderate Re. *Phys. Fluids*, *9*, 3398-3409.

Eggels, J. G. M., Unger, F., Weiss, M. H., Westerweel, J., Adrian, R. J., Friedrich, R., & Nieuwstadt, F. T. M. (1994). Fully developed turbulent pipe flow: a comparison between direct numerical simulation and experiment. *J. Fluid Mech.*, *268*, 175-209.

Hultmark, M., Vallikivi, M., Bailey, S. C. C., & Smits, A. J. (2013). Logarithmic scaling of turbulence in smooth- and rough-wall pipe flow. *J. Fluid Mech.*, *728*, 376-395.

Kähler, C. J., Scholz, U., & Ortmanns, J. (2006). Wall-shear-stress and near-wall turbulence measurements up to single pixel resolution by means of long-distance micro-PIV. *Exp. Fluids*, *41*, 327-341.

McKeon, B. J., Li, J., Jiang, W., Morrison, J. F., & Smits, A. J. (2004). Further observations on the mean velocity distribution in fully developed pipe flow. *J. Fluid Mech.*, *501*, 135-147.

Scharnowski, S., Hain, R., & Kähler, C. J. (2012). Reynolds stress estimation up to single-pixel resolution using PIV-measurements. *Exp. Fluids*, *52*, 985-1002.

Sridharan, S. (2018). *Towards high resolution particle image velocimetry* (Unpublished master's thesis). Technische Universiteit Delft.

Vallikivi, M., Hultmark, M., Bailey, S. C. C., & Smits, A. J. (2011). Turbulence measurements in pipe flow using a nano-scale thermal anemometry probe. *Exp. Fluids*, *51*, 1521-1527.

Vinuesa, R., Duncan, R. D., & Nagib, H. M. (2016). Alternative interpretation of the Superpipe data and motivation for CICLoPE: the effect of a decreasing viscous length scale. *Eur. J. Mech. B-Fluid*, *58*, 109-116.

Westerweel, J. (2008). On velocity gradients in PIV interrogation. *Exp. Fluids*, *44*, 831-842.

Westerweel, J., Geelhoed, P. F., & Lindken, R. (2004). Single-pixel resolution ensemble correlation for micro-PIV applications. *Exp. Fluids*, *37*, 375-384.

Westerweel, J., Petracci, A., Delfos, R., & Hunt, J. C. R. (2011). Characteristics of the turbulent/non-turbulent interface of a non-isothermal jet. *Phil. Trans. R. Soc. A*, *369*, 723-737.

Willert, C. E., Soria, J., Stanislas, M., Klinner, J., Amili, O., Eisfelder, M., … Talamelli, A. (2017). Near-wall statistics of a turbulent pipe flow at shear Reynolds numbers up to 40 000. *J. Fluid Mech.*, *826*, R5.

Wu, X., & Moin, P. (2008). A direct numerical simulation study on the mean velocity characteristics in turbulent pipe flow. *J. Fluid Mech.*, *608*, 81-112.

Zagarola, M. V., & Smits, A. J. (1998). Mean-flow scaling of turbulent pipe flow. *J. Fluid Mech.*, *373*, 33-79.